Journal of Engineering for Gas Turbines and Power. Received August 02, 2023;
Accepted manuscript posted October 16, 2023. doi:10.1115/1.4063773

THE ROLE OF DIFFUSIVE MIXING IN CURRENT AND FUTURE AVIATION FUELS AT RELEVANT OPERATING CONDITIONS

Francesco Di Sabatino, Kevin Wan and Julien Manin
Combustion Research Facility, Sandia National Laboratories
Livermore, CA

Tyler Capil and Yolanda Hicks
NASA Glenn Research Center
Cleveland, OH

Alex Gander and Cyril Crua
Advanced Engineering Centre, University of Brighton
Brighton, UK

ABSTRACT

With aviation's dependence on the high volumetric energy density offered by liquid fuels, Sustainable Aviation Fuels (SAFs) could offer the fastest path towards the decarbonization of aircrafts. However, the chemical properties of SAFs present new challenges, and research is needed to better understand their injection, combustion and emission processes. While efforts such as the United States National Jet Fuel Combustion Program (NJFCP) that investigated several aspects in detail, certain processes were unfortunately beyond the reach of this program. One of them in particular is about droplet evaporation at relevant pressures and temperatures, and this represents the focus of the present manuscript. To address this gap we characterized the evaporation and mixing of spray droplets injected into well-controlled thermodynamic environments at conditions relevant to modern and next generation aero-engine combustors. We tested three fuels from the NJFCP, namely an average Jet A fuel (A-2), an alcohol-to-jet fuel containing highly branched dodecane and hexadecane type components (C-1), and a blend made of 40 % C-1 and 60 % iso-paraffins ranging from 9 to 12 carbon atoms (C-4). We also tested a single component normal alkane: n-dodecane, as well as an advanced bio-derived cyclo-alkane fuel: bicyclohexyl. The time evolution of fuel droplets was monitored using high-speed long-distance microscopy in a specific configuration that enabled sharp images to be acquired at these extreme conditions. The collected images were processed using a purposely-developed and trained machine learning (ML) algorithm to detect and characterize the droplets' evaporation regime. The results revealed different evaporation regimes, such as classical and diffusive. In agreement with previous studies, evaporation regimes appear to be controlled by ambient pressure, temperature, and fuel type. The measurements demonstrate that diffusive evaporation is relevant at high-pressure conditions, such as take-off combustor pressures for modern commercial aircraft engines. However, classical evaporation mostly controls mixing at lower pressure, such as cruise altitude conditions. The ML analysis emphasized that multiple evaporation regimes co-existed at the same operating condition and no significant relationship was found between droplet size and evaporation regime. The findings of this work constitute a database for validating spray and droplet models that are necessary for implementing lower emissions fuels in aero-engines.

Keywords: Droplet evaporation, sustainable aviation fuels, long-distance microscopy, machine learning, diffusive evaporation.

NOMENCLATURE

FWHM	Full width at half maximum
LHV	Lower heating value [MJ/kg]
ML	Machine learning
NJFCP	National jet fuel combustion program
Pc	Critical pressure [bar]
Pr	Reduced pressure (ambient pressure divided by critical pressure)
SAF	Sustainable aviation fuel
SHA	Single-hole atomizer
Tc	Critical temperature [K]
Tr	Reduced temperature (ambient temperature divided by critical temperature)
x	Droplet width based on the bounding box [mm]
y	Droplet height based on the bounding box [mm]

1. INTRODUCTION

Stringent regulations will be implemented in the coming years around the world to reduce harmful emissions from aero-engines [1]. Aviation presently accounts for around 4% of the net radiative forcing, even though there is still ongoing debate on the actual value as well as on the uncertainty of the estimated emission [2]. Climate forcing figures related to aviation are also expected to increase in the coming decades to about 10%, mostly due to the increase in air traffic [3]. In this context, there has been a substantial effort in recent years to develop fuels that would be more climate-friendly than the refined aircraft fuels that have been burnt for over half a century. While the perfect fuel is unlikely to exist, what we refer to as sustainable aviation fuels

(SAFs) represent the next generation of fuels with the aim to reduce the environmental impact of aero-engines [4], [5]. The National Jet Fuel Combustion Program (NJFCP) crafted surrogate fuels aiming at investigating the performance of newly developed SAFs at specific operating conditions, such as cold start, high-altitude relight, and lean-induced flame extinction [4], [6]–[8]. A major effort was also devoted to investigating ignition characteristics and chemical properties of these newly developed fuels. It is important to note that the NJFCP created extremely useful tools for the screening of SAFs and the evaluation of their relevant properties, but relatively small effort was devoted to evaluate more fundamental characteristics, such as soot formation and liquid spray properties [8], [9]. The data presented in Refs. [8] and [9] are of high interest but they are mainly focused on droplets' dimensions and spray breakup.

While a previous publication by the authors quantified flame characteristics and soot formation for several SAFs [10], the present manuscript investigates the evaporation characteristics of spray-generated droplets injected into high-pressure and high-temperature environments. Specifically, the main objective is to characterize the evaporation of droplets during and immediately after injection. This is of particular interest since no studies have been performed at conditions and using fuels relevant to aero-engine combustion, to the authors' knowledge. Historically, transcritical or supercritical mixing is most relevant to rocket engines, where ambient pressure and temperature are well above the critical point of the fuel [11]. With the continuous developments and improvements of combustion systems, these regimes became relevant to compression-ignition engines (i.e. diesel engines), where combustion chamber pressure at injection routinely reaches upward of 10 MPa, with temperature approaching 1000 K. Previous works by the authors delved into such conditions, highlighting the importance of transcritical mixing [12], [13]. For instance, Manin *et al.* [12] analyzed the characteristics of n-dodecane spray droplets at conditions relevant to diesel combustion in a constant-volume pre-burn vessel using high-speed long-distance microscopy. They observed surface tension across a large number of conditions, including many above the critical pressure and temperature of the fuel. However, they noted a loss of surface tension for droplets when operating at conditions well above the critical point. Additionally, they highlighted that the increase in pressure had a significant effect on surface tension, while the increase in temperature had only a minimal impact. In a subsequent campaign, Crua *et al.* [13] investigated droplet evaporation for three alkane fuels under similar conditions. They identified three distinct evaporation regimes:

- Classical: Droplets retain strong surface tension with continuous and progressive heat and mass transfer between liquid phase and gaseous phase. The droplets maintain a spherical shape and d^2 law-based evaporation model can be assumed for these droplets throughout their lifetime [14].
- Transitional: Droplets undergo an initial classical evaporation, followed by a loss of surface tension that leads to accelerated vaporization and stretching of the liquid/gas interface. The droplets transition from a spherical shape to a more stretched and deformed profile.
- Diffusive: Droplets experience a complete (or near complete) loss of surface tension and two-phase flow cannot be assumed anymore. Additionally, droplets are no longer spherical in shape since they oscillate and deform continuously.

From these studies, the authors generated thermodynamic maps to define the controlling conditions for which the evaporation regime shall be considered classical, transitional or diffusive. These findings were also confirmed by others [15], [16]. However, the results of these studies were in opposition to the state-of-the-art models at the time, in which droplet evaporation follows well-established evaporation laws. Crucial work by Dahms et al. [17], [18] proposed new approaches that more accurately described the evaporation regime under these conditions. The developed numerical framework suggests that the interface between the liquid and ambient gases evolves, broadening with time, inducing a reduction in surface tension leading to a breakdown of that same interface. Without strong intermolecular forces at the interface, the liquid-like fluid feature becomes highly challenged by the surrounding aerodynamic forces, allowing the fluids to mix in what resembles a single-phase manner. Recent numerical efforts [19], [20] confirmed not only the importance of transcritical evaporation and mixing over a wide range of applications, but also the range of thermodynamic conditions over which the different regimes are relevant.

Considering the improvements made to aero-engine propulsion, with overall pressure ratios upward of 50 on modern engine technologies, the question arises whether transcritical evaporation is relevant to these combustion systems, as described by Oefelein [21]. As highlighted above, there has been a substantial effort to investigate evaporation and mixing for fuels and at conditions relevant to compression-ignition combustion engines, but to the authors' knowledge, no such studies were carried out for aviation fuels injected into environments matching the conditions inside modern and next generation combustors. Studying relevant fuels at real conditions is necessary to provide fundamental understanding of evaporation regimes in aero-engines, but also guide the development of reliable models.

The present work investigates the evaporation regimes for fuels relevant to aviation in the recent context of SAFs. The fuels were injected into highly controlled environments, emulating a wide range of pressures and temperatures matching the conditions found in modern and next-generation aero-engine combustors. The spray-generated droplets were imaged via a purposely-built optical system able to capture small features of micrometric scales under high pressure and temperature environments. The images were analyzed via a machine learning algorithm to automatically detect and classify the droplets into the evaporation regimes described above.

Journal of Engineering for Gas Turbines and Power. Received August 02, 2023;
Accepted manuscript posted October 16, 2023. doi:10.1115/1.4063773

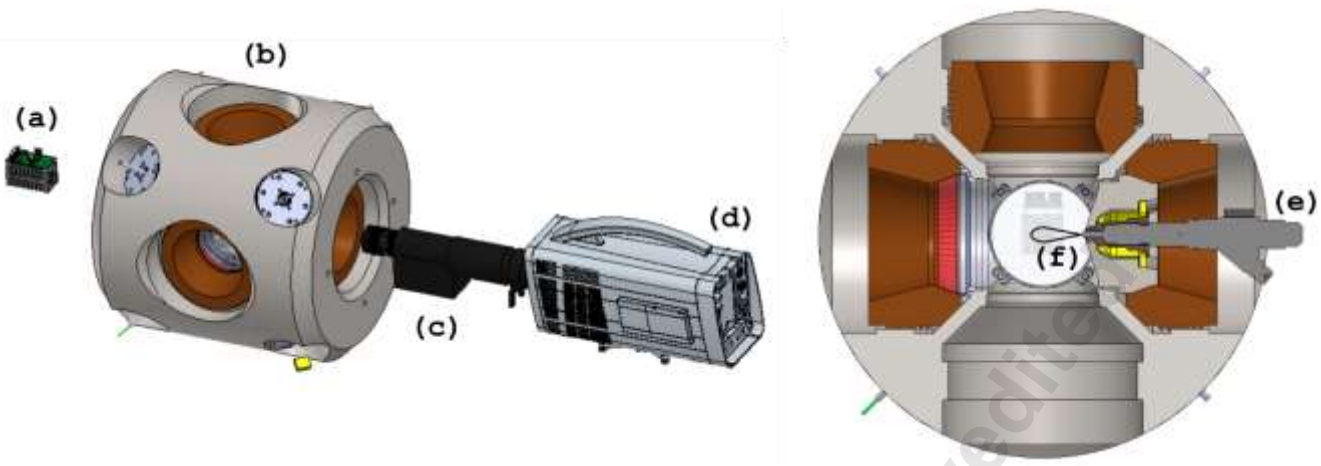

FIGURE 1: A SCHEMATIC OF THE EXPERIMENTAL SETUP (LEFT) AND A CROSS-SECTIONAL VIEW OF THE COMBUSTION CHAMBER (RIGTH). THE HIGH-SPEED LED SYSTEM (a), THE OPTICAL-ACCESSIBLE CONSTANT VOLUME VESSEL (b), THE LONG-DISTANCE MICROSCOPE (c), THE HIGH-SPEED CAMERA (d), THE SHA (e), AND A CARTOON OF THE SPRAY PLUME (f) ARE SHOWN. DIMENSIONS ARE NOT TO SCALE.

2. EXPERIMENTAL SETUP AND PROCEDURE

The experimental setup used and the experimental procedure followed in this work are described in this section. First, the Sandia constant volume pre-burn combustion vessel is described, together with the injection system and operating conditions. Second, the optical diagnostics used to investigate droplet evaporation is presented. Lastly, the experimental procedure followed to perform experiments and collect data, as well as the methods to classify the evaporation regime of the droplets are presented.

2.1 Experimental setup and conditions

The fuel sprays were injected into a constant-volume pre-burn combustion vessel. The injection system was composed of a high-precision syringe pump (Teledyne 30D) to pressurize the fuel, while the injector was a custom solenoid-actuated injector that we call the single-hole atomizer (SHA). The SHA features a single-hole nozzle with a measured diameter of 175 μm, and it can operate over a wide range of injection pressure conditions, from atmospheric up to 350 bar. Being a solenoid-actuated injector, the SHA differs from continuous flow injectors that are found in aero-engines combustors. However, the objective of this manuscript is to investigate the underlying physics of evaporation regime between different fuels at engine relevant conditions. Therefore, the dissimilarities between the SHA and a real aero-engine injector in terms of atomization and evaporation are expected to be minimal for the scope of this paper. Additional information on the relevance of the SHA-based analysis of phenomena in aero-engines combustors can be found in [22].

The thermodynamic conditions in the constant-volume vessel are reached by spark-igniting a mixture of combustible gases. The target conditions are met following a rapid increase in pressure and temperature, and a cooldown process that typically is several seconds long, determined by the energy balance between the charge gas enthalpy and the heat transfer to the vessel system. The facility can emulate thermodynamic conditions as high as 355 bar and 1800 K. Depending on the pre-burn mixture, oxygen concentrations can range from 0 to 21%. Additional information about the chamber and its operation can be found in Ref. [23]. A schematic of the vessel is shown in Fig. 1.

Two ambient pressures were selected, one corresponding to combustor pressures representative of take-off conditions (60 bar), and another more characteristic of cruise conditions (20 bar). The ambient temperature was varied between 900 and 1700 K. This range of temperatures was selected to be representative of conditions that could be found in aero-engine combustors. Since this work was focused on droplet evaporation, and to have a better control on ambient temperature, these experiments were performed under inert conditions (0 % oxygen concentration). Even though the temperature and pressure conditions were representative of operating conditions of aero-engines, the absence of other phenomena such as the presence of the flame or the swirling flow could affect the droplets evaporation process. However, the main objective of this work is to investigate droplet evaporation decoupled from any other phenomenon.

The fuels investigated in this work and their respective critical pressure and temperature, density and lower heating value (LHV), estimated from correlations and data from [6], [24]–[28] are reported in Tab. 1. Other fuel properties that would be relevant to this study, such as viscosity or surface tensions were not available for all fuels, as well as at relevant conditions for this paper, and were therefore not listed. An interested reader can refer to [28]–[30] for viscosity and surface tension values at substantially lower temperature for fuels investigated in this work.

Considering the fuels reported in Tab. 1, A-2 is refined Jet-A fuel with average characteristics. C-1 is an alcohol-to-jet fuel containing highly branched dodecane and hexadecane type components, while C-4 is a blend made of 40 % C-1 and 60 % iso-paraffins ranging from 9 to 12 carbon atoms [9], [31].

Journal of Engineering for Gas Turbines and Power. Received August 02, 2023;
Accepted manuscript posted October 16, 2023. doi:10.1115/1.4063773
Section 3 and 1 shared copyright

Bicyclohexyl, a bio-derived cyclo-alkane fuel was also tested [4], [5], [32]. Last, n-dodecane (nC12) was also studied since it has been a logical surrogate choice for jet fuel, and detailed/reliable kinetic mechanisms are available [4], [5], [33]. A multi-component diesel fuel surrogate (CRC V2) was also added for comparison and to provide a frame of reference with respect to previous works. The density and LHV listed in Tab. 1 were taken from Mueller et al. [32], while critical properties were computed using the mole-weighted critical point for the different components. Note that critical properties for diesel fuel have been published by others (see Lin and Tavlarides [34] for example), but the V2 surrogate crafted by the CRC AVFL-18a panel matches a broad range of properties of certification diesel fuel.

TABLE 1: LIST OF FUELS INVESTIGATED AND THEIR CRITICAL PRESSURE AND TEMPERATURE, AS WELL AS DENSITY AT 20°C, AND LHV. DIESEL FUEL, NOT INVESTIGATED IN THIS WORK, HAS BEEN REPORTED FOR COMPARISON.

FUEL	NJFCP NAME	Pc [bar]	Tc [K]	Density at 20°C [kg/m^3]	LHV [MJ/kg]
Jet A	A-2	21.2	665	800	43.1
C-1	C-1	19.9	640	760	43.9
C-4	C-4	20.6	627	759	43.8
Bicyclohexyl	-	26.1	745	886	43.4
n-Dodecane	-	18.2	658	750	44.1
Diesel (V2)	-	22.9	728	853	42.5

The injection pressure was set to 30 or 70 bar, depending on the chamber pressure, in order to maintain a 10-bar pressure difference. The injection duration was set to 1 ms to have a proper analysis of the evaporation characteristics of the droplets. In this case, the short injection reduced the effect of evaporation cooling on the charge gas, thereby limiting the drop in local temperature. This is important as the analysis is based on the temperature into which the droplets are injected and travel. Larger amounts of fuel would cool the air-fuel mixture and inevitably bias the analysis.

2.2 Optical diagnostics

A schematic of the optical setup implemented in this work is shown in the left part of Fig. 1. A high-speed camera (iX Cameras iSpeed 727) equipped with a long-distance microscope (Infinity K2-DistaMax) was used to collect images of the droplet evaporation process and regime at 5 kHz frame rate. The long-distance microscope lens was configured with a CF-2 objective, and NTX 2x magnifier to achieve the desired digital resolution. Non-uniform illumination intensities and beam-steering were reduced using a line-of-sight illumination configuration with diffuse lighting [12].

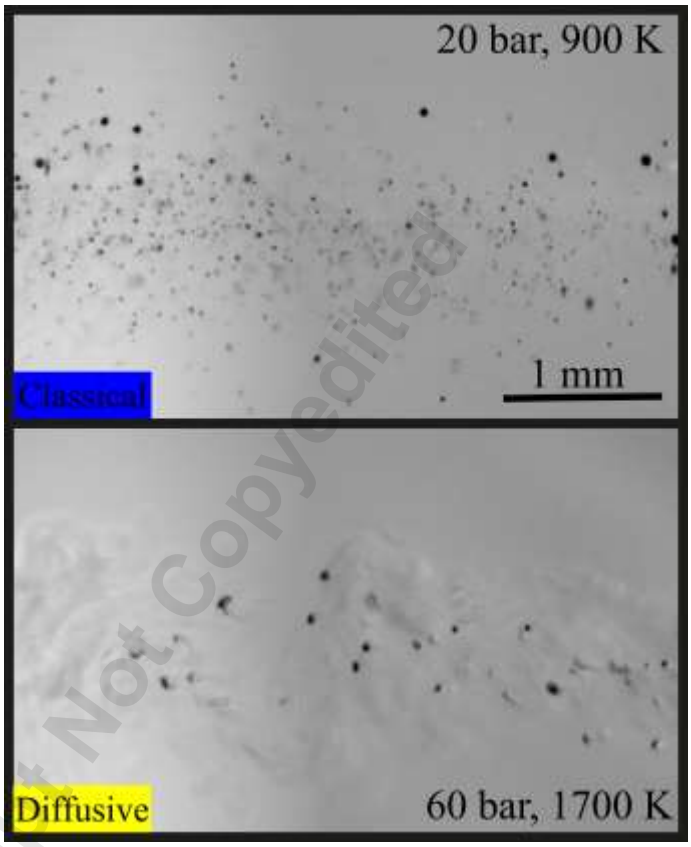

FIGURE 2: EXAMPLES OF IMAGES COLLECTED WITH LONG-DISTANCE MICROSCOPY FOR n-DODECANE FUEL. CLASSICAL EVAPORATION REGIME ON TOP, DIFFUSIVE EVAPORATION REGIME ON THE BOTTOM. TEMPERATURE AND PRESSURE OF THE SPECIFIC CONDITION ARE ALSO REPORTED.

A custom LED system producing pulses of light at 450 nm (20 nm FWHM) for 250 ns at 5 kHz was used. The LED illumination was collected and collimated using a set of condenser lenses, and directed onto a custom engineered diffuser to produce a controlled and efficient pseudo-Lambertian illumination. The system's digital resolution at the object plane was 3.77 µm/pix, which with the 2072 × 1536 pix^2 sensor, resulted in a field of view on the order of 7.8 x 5.8 mm^2.

2.3 Experimental procedure

The high-speed imaging system allowed hundreds of images of droplet evaporation to be collected at each operating condition. However, only isolated droplets were analyzed to properly distinguish the evaporation process. Figure 2 shows examples of images acquired by the microscopy system for n-dodecane fuel under two ambient conditions. Three to five repetitions were performed at each operating condition to ensure reproducibility of the results and collect statistics.

Journal of Engineering for Gas Turbines and Power. Received August 02, 2023;
Accepted manuscript posted October 16, 2023. doi:10.1115/1.4063773
Section 3 and 1 shared copyright

2.4 Images post-processing and classification of evaporation regime

Image post-processing was only used to remove intensity gradients caused by non-homogeneous backlighting: all frames were flat-fielded using the first frames (prior to injection) from each sequence.

Samples from two separate datasets were then manually labelled to provide training and validation images for a machine learning algorithm: the 'ALKANE' dataset published in [13], and the 'SAF' dataset presented in this article. Both datasets used similar (but not identical) experimental setups. In both instances the droplets were labelled as either 'classical' or 'diffusive', following the definitions introduced in [13]. It should be noted that while three evaporation regimes were identified in previous works, it was decided for the purpose of this current project to limit the analysis to classical and diffusive regimes only. A total of 577 droplets were individually labelled, with 164 from the ALKANE set, and 413 droplets from the SAF set. Both labelled datasets were then split for training and validation. Training the ML algorithm with 577 droplets may not be sufficient to guarantee reliable results. It is also worth adding that the droplets used to train the algorithm were assessed by visual inspection, meaning that there could be a subjective bias included in the data used for training. To limit this potential bias, the training data were labelled by two team members with the most experience of high-speed visualizations of transcritical mixing.

In order to automate the analysis of the full SAF dataset, we used both datasets to train YOLOv5, a state-of-the-art single-stage object detection algorithm that uses a deep convolutional neural network. We selected YOLOv5 for its accuracy and speed, as well as its ability to achieve multi-scale prediction. Speed was essential due to the size of the dataset (~25,000 frames at 2072 × 1536 pix^2), while multi-scale resilience was necessary to track the evolution of evaporating droplets through time. The network architecture of YOLOv5 comprises a CSP-Darknet53 backbone to extract features from the input images, a PANet neck to generalize objects of different scales, and the YOLO layer as the model's head to output the object bounding boxes, classes, and scores.

Training was performed on a hybrid cluster using a mix of CPUs and GPUs. The ML tasks were mostly performed on the GPU side, which consisted of Quadro P6000 cards. It took approximately 20 hours for the training to be completed. A genetic algorithm was used to optimize the model's hyperparameters, including learning rate, image rotation, scale, mirroring and hue. To retain certain essential morphological features of the droplets (e.g. sphericity of droplets undergoing a classical evaporation regime) we prevented any change/optimization of the image perspective and shear. The best evolution was fine-tuned for 20,000 epochs on the combined ALKANE and SAF datasets. The best epoch's weights were then used to analyze the full SAF dataset. Example of droplets detected by the machine learning algorithm are reported in Fig. 3. Only results with a confidence value above 50% are considered and presented in this manuscript.

To validate the ML results, and offer comparisons to past efforts, a visual inspection of the high-speed images was also performed to identify the evaporation regime at all conditions. As a human-based approach, the results of this inspection are not as resolved as the classification provided by the ML algorithm. A three-star system was adopted to classify the images. The color of the stars defines the evaporation regime: blue for classical and yellow for diffusive. These stars are reported on the side of the graphs presented in Figs. 4 and 6. Two stars of the same color represent the case where most of the droplets featured a specific evaporation regime, while three same color-filling stars mean that all droplets were in a specific evaporation regime.

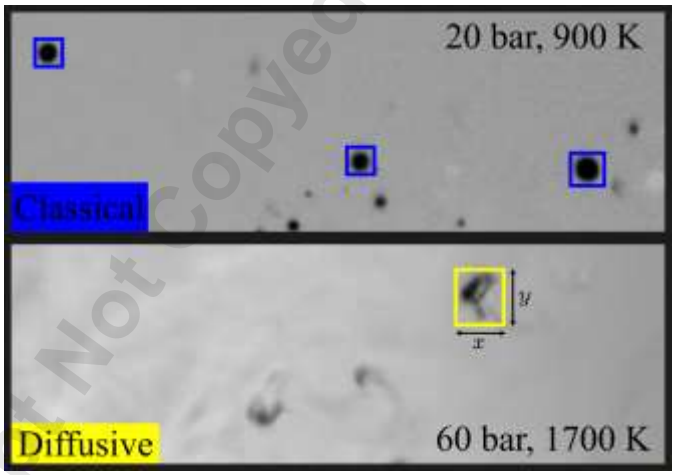

FIGURE 3: EXAMPLES OF DROPLET DETECTED BY THE ML ALGORITHM FOR n-DODECANE FUEL. CLASSICAL EVAPORATION REGIME ON TOP, DIFFUSIVE EVAPORATION REGIME ON THE BOTTOM. X AND Y REPRESENTS THE WIDTH AND HEIGHT OF THE BOUNDING BOX SURROUNDING THE DROPLET. TEMPERATURE AND PRESSURE OF THE SPECIFIC CONDITION ARE ALSO REPORTED.

3. RESULTS AND DISCUSSION

The results of the classification of droplet evaporation regimes are presented and discussed in this section. The results for the lower ambient pressure conditions (20 bar) are shown and discussed first, followed by the higher pressure points (60 bar).

3.1 Evaporation regime and droplet size at cruise conditions

The normalized droplet count for all fuels at cruise conditions is reported in Fig. 4 (left panel). At 20 bar, all fuels mostly exhibited the typical behavior expected in the classical evaporation regime at all temperatures investigated. Note that some temperatures are missing in Fig. 4, mostly because the lower pressure conditions presented limited interest for this experimental campaign and intermediate temperatures were not always tested.

Journal of Engineering for Gas Turbines and Power. Received August 02, 2023;
Accepted manuscript posted October 16, 2023. doi:10.1115/1.4063773

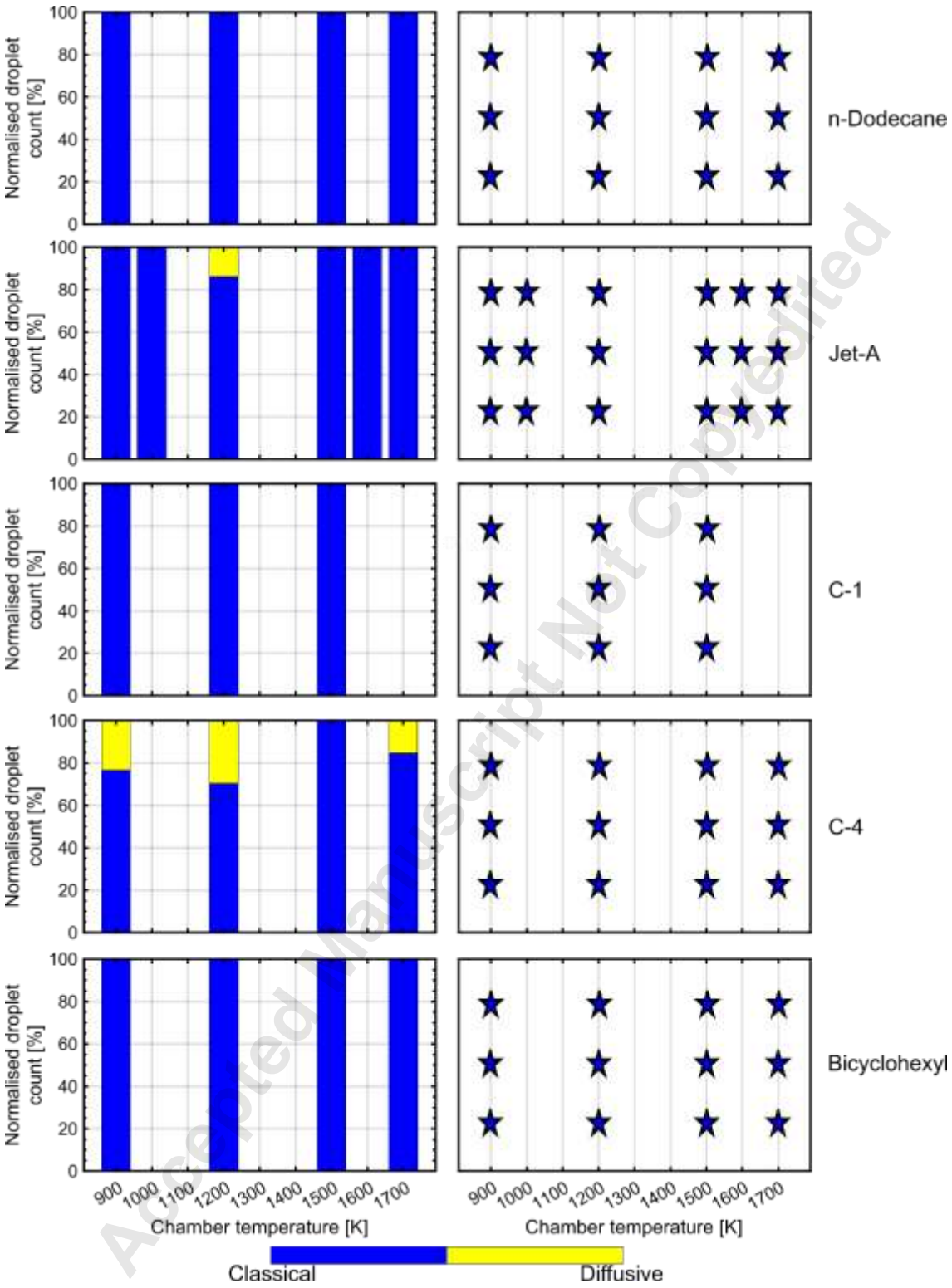

FIGURE 4: NORMALIZED DROPLET COUNT AND EVAPORATION REGIME (LEFT) AND RESULTS OF VISUAL INSPECTION (RIGHT) (BLUE FOR CLASSICAL, YELLOW FOR DIFFUSIVE) FOR ALL FUELS AT 20 BAR OPERATING CONDITIONS. TWO SAME COLOR-FILLING STARS REPRESENT THE CASE WHERE MOST OF THE DROPLETS FEATURED A SPECIFIC EVAPORATION REGIME, WHILE THREE SAME COLOR-FILLING STARS MEANS THAN ALL DROPLETS WERE IN A SPECIFIC EVAPORATION REGIME.

Journal of Engineering for Gas Turbines and Power. Received August 02, 2023;
Accepted manuscript posted October 16, 2023. doi:10.1115/1.4063773
Section 3 and 1 shared copyright

In a few instances, the detection scheme of the ML algorithm did not detect and classify droplets with enough confidence to provide a reliable measure of the classical vs. diffusive fraction; this is why no data was reported for C-1 fuel at 1700 K. Additionally, we mainly focused on four temperature conditions at 20 bar, based on previous experience with n-dodecane. We added additional temperatures for Jet-A due to its composition that consists of species that span carbon numbers from C7 to C18.

The main observation about Fig. 4 is that diffusive evaporation was only detected by the ML algorithm in a few cases at this pressure condition, namely for C-4 at 900, 1200, and 1700 K, and Jet-A at 1200 K. This is certainly due to uncertainties in the droplet classification scheme of the ML algorithm that were exacerbated by multi-dimensional aspects, such as droplets being out of focus, or anisotropy in the illumination due to beam steering. The visual inspection of the images confirmed that all droplets at all conditions were evaporating in a classical fashion (see right panel of Fig. 4). The relatively low pressure, in the vicinity of the critical pressure of the fuels (see Tab.1), might explain why the evaporation regime was classified as classical for nearly all droplets.

To better verify that only the classical evaporation regime was expected for these fuels at these operating conditions, the formulas defined in [13] and shown in Eq. 1 and 2 are applied.

$$T_r\sqrt{P_r} \leq 3.3 \rightarrow classical \quad (1)$$

$$T_r\sqrt{P_r} \geq 3.7 \rightarrow diffusive \quad (2)$$

Where T_r and P_r are the reduced temperature and pressure, the temperature and pressure relative to the critical point of the fuel. At these operating conditions, Eq. 1 was satisfied for all fuels, with values ranging from 1.1 to 2.7, so well below 3.3.

The ML algorithm was also used to obtain information on droplet size at each operating conditions, as reported in Fig. 5. The droplet size parameter, presented in Fig. 5, was defined as the equivalent circle diameter based on the area of the ellipse inscribed in the bounding box defined by x and y (see Fig. 3). Therefore, the computed droplet diameters are expected to be overestimated for test conditions that lead to significant deformations, as it is often the case for transitional or diffusive evaporation regimes. Increasing ambient temperature resulted in fewer droplets being detected as a result of the expected increased evaporation rate. Interestingly, no relationship between droplet size and evaporation regime was observed. Based on previous findings [13], one would expect smaller droplets to undergo diffusive evaporation quicker compared to larger droplets because of the more rapid temperature increase. This was not evident at these operating conditions where nearly all droplets followed the classical evaporation regime. Note that only relatively large droplets are reported since better performance by the ML algorithm was observed for larger drops.

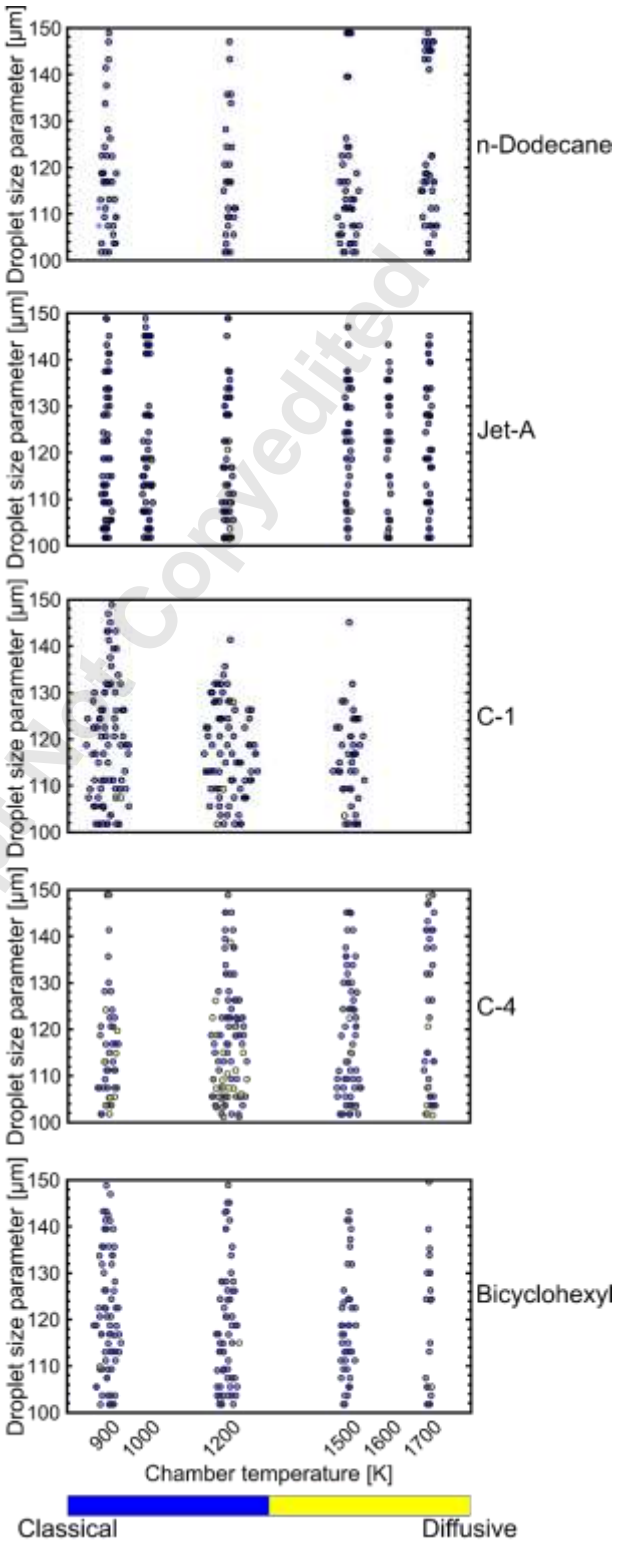

FIGURE 5: DROPLET SIZE PARAMETER AND EVAPORATION REGIME FOR ALL FUELS AT 20 BAR OPERATING CONDITIONS AS DETERMINED BY ML. SPREAD WAS ADDED TO THE DATA POINTS ON THE X-AXIS TO BETTER HIGHLIGHT THE DISTRIBUTION OF DATA ALONG CONCENTRATED AREAS.

Journal of Engineering for Gas Turbines and Power. Received August 02, 2023;
Accepted manuscript posted October 16, 2023. doi:10.1115/1.4063773
Section 3 and 1 shared copyright

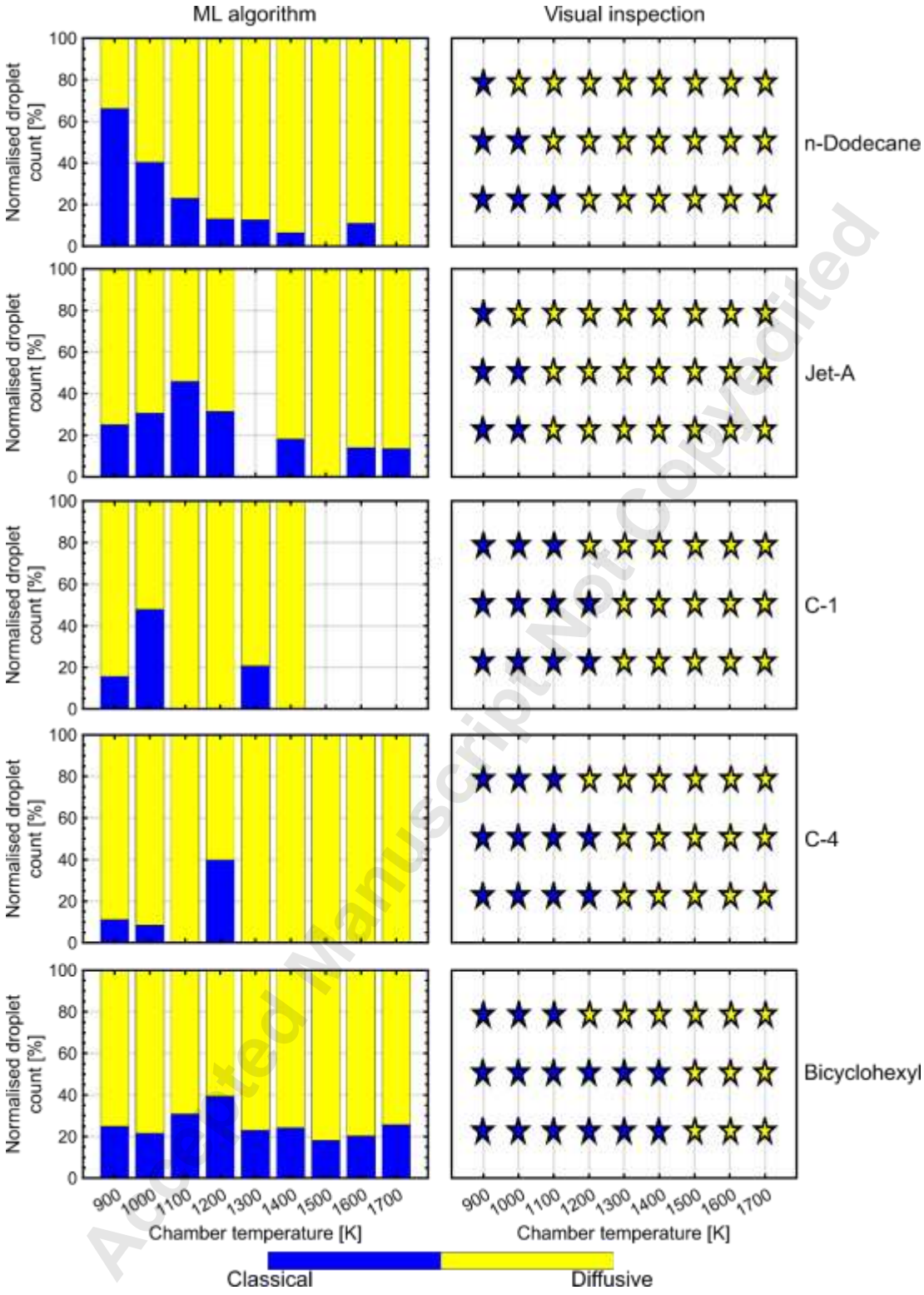

FIGURE 6: NORMALIZED DROPLET COUNT AND EVAPORATION REGIME (LEFT) AND RESULTS OF VISUAL INSPECTION (RIGHT) (BLUE FOR CLASSICAL, YELLOW FOR DIFFUSIVE) FOR ALL FUELS AT 60 BAR OPERATING CONDITIONS. TWO SAME COLOR-FILLING STARS REPRESENT THE CASE WHERE MOST OF THE DROPLETS FEATURED A SPECIFIC EVAPORATION REGIME, WHILE THREE SAME COLOR-FILLING STARS MEANS THAN ALL DROPLETS WERE IN A SPECIFIC EVAPORATION REGIME.

Journal of Engineering for Gas Turbines and Power. Received August 02, 2023;
Accepted manuscript posted October 16, 2023. doi:10.1115/1.4063773
Section 3 and 1 shared copyright

As such, no information for droplets with size parameter lower than 100 µm is reported. It should be noted that the ML algorithm detected and measured the size parameter of droplets smaller than 100 µm, but the level of confidence of the measurements was not high enough for the results to be considered in this work. Limiting the size of the droplets considered for the analysis was also employed as a way to limit the effect of the differences between fuels in terms of fluid physical properties, such as surface tension and viscosity. These parameters are known to affect atomization and a fortiori droplet size, which, if not controlled, may bias the results of the regime classification. Note that it is expected for modern atomizers in real aero-engines combustors to produce droplet size distributions mostly centered below 100 µm. We remind the reader that the size parameter overestimates the actual droplet diameter. Nevertheless, future work will focus on improving the ML methods to detect and more reliably classify droplets over a more relevant size range.

3.2 Evaporation regime and droplet size at take-off conditions

The normalized droplet count for all fuels at take-off conditions (60 bar) is reported in the left panel of Fig. 6. As previously mentioned, some fuels have data missing at specific temperatures due to the classification confidence threshold provided by the ML algorithm. At higher pressure conditions, there was an obvious transition from classical to diffusive evaporation with increasing temperature for all fuels due to the ambient conditions being substantially higher than the critical temperature and pressure (see Tab.1). Contrary to what was observed at cruise conditions, different behaviors were observed with respect to the classified evaporation regime as temperature increased. In a way similar to what was done for the cruise data, the results coming from the visual inspection, using the three-star system, are reported for each fuel and each temperature in the right panel of Fig. 6. Contrasting with the results of Fig. 4, where visual inspection determined that all droplets evaporated following the classical regime for all temperatures investigated, the visual inspection at 60 bar showed changing regimes across the range of temperatures tested.

The classification produced by the ML analysis for n-dodecane showed an increasing number of droplets in the diffusive evaporation regime with increasing temperature. The ML data and the results of the visual inspections are in reasonable agreement, with near complete transition to diffusive evaporation around 1200-1300 K for both approaches, despite the fact that the ML algorithm still showed few droplets evaporating in a classical fashion between 1200 and 1600 K. Applying Eq. 2 at these conditions resulted in values between 2.3 and 4.3 for n-dodecane, with values above 3.7 obtained above 1300 K, supporting the results of the ML-produced classification as well as the visual inspection.

On the other hand, the ML results and the visual inspection are not in good agreement for Jet A. Specifically, the visual inspection suggested that the transition to diffusive evaporation occurred around 1100 K, while the ML algorithm presented droplets in classical evaporation regime even at 1700 K.

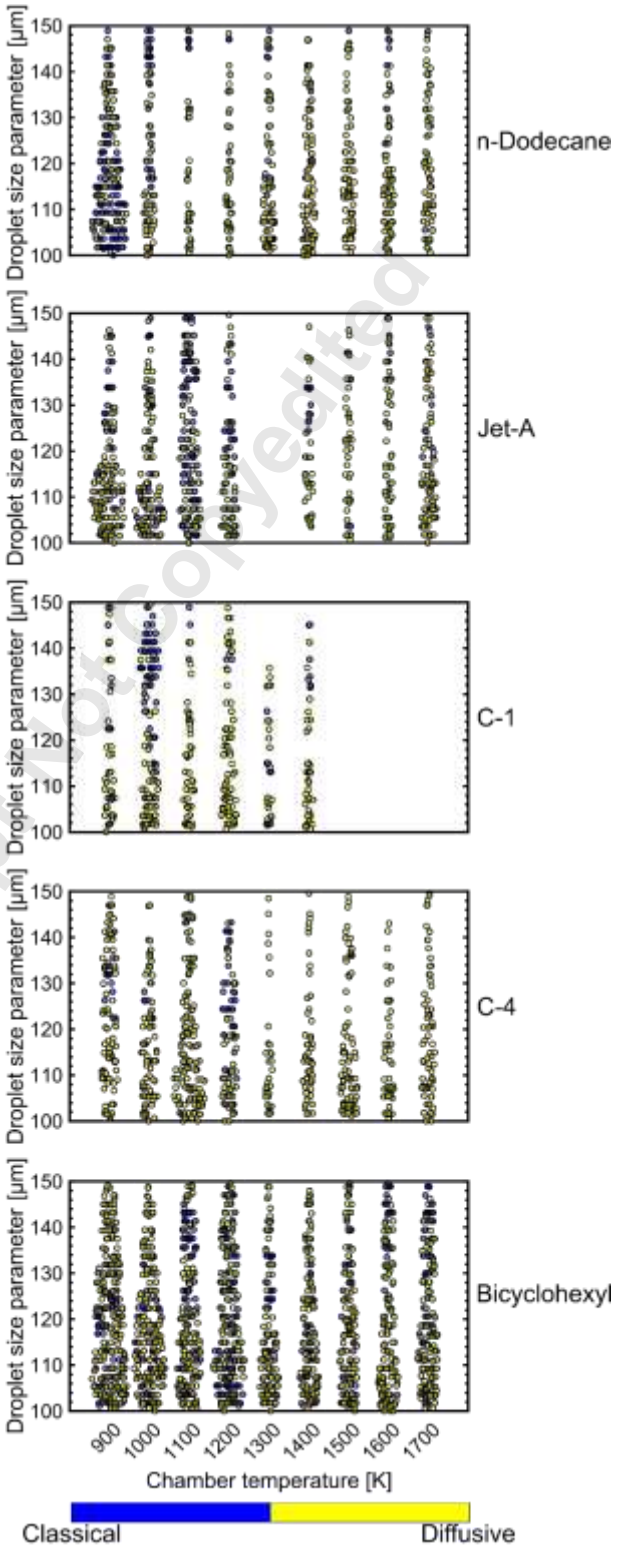

FIGURE 7: DROPLET SIZE PARAMETER AND EVAPORATION REGIME FOR ALL FUELS AT 60 BAR OPERATING CONDITIONS AS DETERMINED BY ML. SPREAD WAS ADDED TO THE DATA POINTS ON THE X-AXIS TO BETTER HIGHLIGHT THE DISTRIBUTION OF DATA ALONG CONCENTRATED AREAS.

Journal of Engineering for Gas Turbines and Power. Received August 02, 2023;
Accepted manuscript posted October 16, 2023. doi:10.1115/1.4063773
Section 3 and 1 shared copyright

Interestingly, and against expectations, is the fact that the fraction of droplets with classical evaporation regime did not seem to decrease monotonically, as was observed with n-dodecane. In this case, applying Eq. 2 to Jet-A suggests a fully diffusive regime above 1400 K. The visual inspection pointed towards an evaporation process dominated by the diffusive regime at lower temperature, near 1100 K and above. Additional analyses will be performed to better investigate this fuel.

C-1 and C-4 also showed disagreement between the results from the ML processing and the visual inspection. The visual inspection suggested that the transition to diffusive evaporation occurs around 1300 K, with a very well-matched behavior for both fuels. Both fuels showed few droplets with classical evaporation regime at 1300 K. The non-monotonic aspect of the trend certainly highlights a degree of uncertainty in the ML processing. The empirical model of Eq. 2 suggested that both C-1 and C-4 can be expected to transition to a diffusive-dominated regime at temperatures near 1300 K.

Bicyclohexyl exhibited a behavior that required substantially higher temperatures than the other fuels to enter the diffusive evaporation regime. The visual inspection suggested that the transition temperature was closer to 1500 K. This trend might be due to the higher critical temperature and pressure compared to the other fuels (see Tab.1). While there was no major disagreement between the ML processing and the visual inspection, the fairly constant fraction of droplets evaporating following the classical or diffusive regimes from the ML processing was unexpected based on our experience. Bicyclohexyl features values between 1.8 and 3.5 from Eq. 2, supporting its resistance to diffusive evaporation, as hinted by the visual inspection.

Overall, the results produced by the visual inspection approach were more in agreement with the expectations following the empirical correlations given in Eq. 2 compared to the ML-processed results. Aspects described earlier about the potential shortcomings related to the training of the ML method bear importance regarding the certainty of the ML output. Nevertheless, the ML processing produced reasonable results for essentially all cruise conditions, as well as for certain high-pressure conditions, highlight the potential of the ML approach. It is important to note that while the ML algorithms may fail at accurately describing the evaporation regime across a wide range of fuels and temperatures, this exercise highlighted the fact that evaporation under these conditions is not only dualistic. On the contrary, many experiments featured a mix of evaporation regimes, with droplets evaporating in a classical way, and others undergoing an evaporation process where diffusive mixing dominated. The co-existence of different regimes of evaporation is extremely important in the context of numerical simulations of spray atomization and mixing, leading to combustion.

The size parameters of the droplets detected by the ML algorithm are reported in Fig. 7 for all fuels and temperatures at 60 bar ambient pressure. Note again that only relatively large droplets were analyzed by the ML algorithm so no information could be extracted for droplets with size parameter lower than 100 µm. As was mentioned after Fig. 5, fewer droplets were being detected with increasing temperature, since fewer droplets were present overall. It was even more obvious at these operating conditions that no relation between droplet size and evaporation regime existed for these fuels. In contrast with the results at cruise conditions, all fuels showed both evaporation regimes for the entire range of size parameter of droplets investigated in this manuscript.

4. CONCLUSION

This manuscript presented the results of an experimental study looking into the evaporation regimes of liquid droplets of current and some NJFCP reference jet fuels at conditions relevant to aero-engine combustors, and above the critical point of the fuels. A non-continuous injection strategy which used a single-hole nozzle injector (called the single-hole atomizer, or SHA) was implemented to generate fuel sprays into a quiescent environment at well-controlled thermodynamic conditions, relevant to modern or next generation aero-engines. Five fuels, A-2 (Jet A), C-1, and C-4 from the NJFCP fuel matrix, an advanced bio-derived cyclo-alkane (bicyclohexyl) as well as n-dodecane have been investigated.

Two ambient pressures have been tested: 20 and 60 bar, to represent cruise altitude as well as take-off conditions, respectively. The environment was inert to prevent combustion, and the ambient temperature was adjusted between 900 and 1700 K to cover a wide range of temperature conditions. The optical access provided by the constant volume vessel utilized in this work allowed the implementation of high-speed long-distance microscopy to image the time evolution of spray droplets. A machine-learning algorithm was implemented to detect droplets and to assess their evaporation regime. The results of this algorithm were verified by direct visual inspection of the acquired images. The main findings of this work are summarized in the following:

- Classical and diffusive evaporation regimes were observed to co-exist at the same operating condition. Therefore, not every single droplet was undergoing the same evaporation regime at the same operating conditions. This result has strong implication for numerical simulations, since a single evaporation regime at a specific operating condition cannot be assumed;
- The comparison between ML and visual inspection results showed that the algorithm performed well at cruise conditions, where the classical evaporation regime dominated, but that substantial differences were observed at higher (take-off) ambient pressure. This highlights the need for the ML algorithm to be improved to properly detect the droplets and classify the evaporation regime with confidence.
- The ML classification shows no relationship between droplet size and evaporation regime. However, only relatively large droplets were considered, since the confidence value of droplet size parameters for smaller

droplets where below the 50% threshold imposed in this investigation.

- The results confirm the pertinence of the empirical formulas proposed by Crua et al. [13] to the fuels and conditions applied in the present work.
- The measurements demonstrate that diffusive mixing is present for all investigated fuels at take-off. Therefore, it is important to consider this regime when simulating spray behavior in aero-engine combustors.
- The results highlight different evaporation regime boundaries between current and future jet fuels. The difference is expected to have a direct impact on the mixing process and all processes connected to mixing, such as flame stabilization and soot production.

Overall, the data presented in this paper constitute valuable information regarding droplet evaporation towards the development and/or validation of models relevant to evaporation and mixing in aero-engine combustors. Future work will attempt to draw correlations between evaporation regime and evaporation rate to further improve evaporation models at pressures and temperatures above the critical point of fuels. It is also important to stress again that the ML approach provided reliable information for several conditions, but not across the whole test matrix. Ongoing efforts focus on refining the ML technique such that it can be applied to a broader range of operating conditions and fuels.

ACKNOWLEDGEMENTS

The authors would like to thank Dr. Eric Mayhew at the Army Research Laboratory for supplying the fuels, as well as Kyra Schmidt at Sandia National Laboratories for her dedicated support of the Spray Combustion Laboratory. This research was supported by the U.S. Department of Energy (DOE) Office of Vehicle Technologies, and was performed at Sandia Nat. Labs in Livermore, CA.

This article has been authored by an employee of National Technology & Engineering Solutions of Sandia,LLC under Contract No. DE-NA0003525 with the U.S. Department of Energy (DOE). The employee owns all right,title and interest in and to the article and is solely responsible for its contents. The United States Governmentretains and the publisher, by accepting the article for publication, acknowledges that the United States Governmentretains a non-exclusive, paid-up, irrevocable, world-wide license to publish or reproduce the published form of thisarticle or allow others to do so, for United States Government purposes. The DOE will provide public access to these results of federally sponsored research in accordance with the DOE Public Access Plan https://www.energy.gov/downloads/doe-public-access-plan. Additional support was provided by the NASA Aeronautics Research Mission Directorate Transformational Tools and Technologies Project.

REFERENCES

[1] M. B. Colket, "Particulate Formation," in *Gas Turbine Emissions*, T. C. Lieuwen and V. Yang, Eds. Cambridge: Cambridge University Press, 2013, pp. 123–153. doi: 10.1017/CBO9781139015462.009.

[2] D. S. Lee *et al.*, "The contribution of global aviation to anthropogenic climate forcing for 2000 to 2018," *Atmos. Environ.*, vol. 244, p. 117834, 2021.

[3] D. S. Lee *et al.*, "Aviation and global climate change in the 21st century," *Atmos. Environ.*, vol. 43, no. 22–23, pp. 3520–3537, 2009.

[4] J. S. Heyne *et al.*, "Year 3 of the national jet fuels combustion program: practical and scientific impacts of alternative jet fuel research," in *2018 AIAA Aerospace Sciences Meeting*, 2018, p. 1667.

[5] J. Heyne, B. Rauch, P. Le Clercq, and M. Colket, "Sustainable aviation fuel prescreening tools and procedures," *Fuel*, vol. 290, p. 120004, 2021.

[6] M. Colket *et al.*, "Overview of the national jet fuels combustion program," *AiAA J.*, vol. 55, no. 4, pp. 1087–1104, 2017.

[7] J. S. Heyne *et al.*, "Year 2 of the National jet fuels combustion program: Towards a streamlined alternative jet fuels certification process," in *55th AIAA Aerospace Sciences Meeting*, 2017, p. 0145.

[8] E. Mayhew *et al.*, "Spray characteristics and flame structure of Jet A and alternative jet fuels," in *55th AIAA Aerospace Sciences Meeting*, 2017, p. 0148.

[9] E. Mayhew *et al.*, "High-speed phase contrast imaging of spray breakup of jet fuels under combusting conditions," *At. Sprays*, vol. 31, no. 1, 2021.

[10] F. Di Sabatino, K. Wan, and J. Manin, "Single-Hole Atomizer (SHA) Research: A New Way to Study Spray Flame Dynamics and Soot Formation for Aero-engine Combustion," *2023 AIAA SciTech Forum and Exposition*.

[11] B. Chehroudi, "Recent experimental efforts on high-pressure supercritical injection for liquid rockets and their implications," *Int. J. Aerosp. Eng.*, vol. 2012, 2012.

[12] J. Manin, M. Bardi, L. M. Pickett, R. N. Dahms, and J. C. Oefelein, "Microscopic investigation of the atomization and mixing processes of diesel sprays injected into high pressure and temperature environments," *Fuel*, vol. 134, pp. 531–543, 2014.

[13] C. Crua, J. Manin, and L. M. Pickett, "On the transcritical mixing of fuels at diesel engine conditions," *Fuel*, vol. 208, pp. 535–548, 2017.

[14] G. M. Faeth, "Current status of droplet and liquid combustion," *Prog. Energy Combust. Sci.*, vol. 3, no. 4, pp. 191–224, 1977.

[15] Z. Falgout, M. Rahm, D. Sedarsky, and M. Linne, "Gas/fuel jet interfaces under high pressures and temperatures," *Fuel*, vol. 168, pp. 14–21, 2016.

[16] M. Wensing, T. Vogel, and G. Götz, "Transition of diesel spray to a supercritical state under engine conditions," *Int. J. Engine Res.*, vol. 17, no. 1, pp. 108–119, 2016.

[17] R. N. Dahms, J. Manin, L. M. Pickett, and J. C. Oefelein, "Understanding high-pressure gas-liquid interface phenomena in diesel engines," *Proc. Combust. Inst.*, vol. 34, no. 1, pp. 1667–1675, 2013.

[18] R. N. Dahms, "Understanding the breakdown of classic two-phase theory and spray atomization at engine-relevant conditions," *Phys. Fluids*, vol. 28, no. 4, p. 042108, 2016.
[19] S. Shariatnia, A. Asadi, and D. Jarrahbashi, "Experimental analysis of supercritical-assisted atomization," *Phys. Fluids*, vol. 33, no. 1, p. 013314, 2021.
[20] S. Xie, Y. Fu, P. Yi, T. Li, and R. Chen, "Evaluation of trans-critical transition of single-and multi-component sprays under diesel engine-like conditions," *Appl. Therm. Eng.*, vol. 202, p. 117830, 2022.
[21] J. C. Oefelein, "Advances in modeling supercritical fluid behavior and combustion in high-pressure propulsion systems," in *AIAA Scitech 2019 Forum*, 2019, p. 0634.
[22] L. M. Pickett, J. Manin, F. Di Sabatino, T. Nguyen, and S. Kook, "Mimicking gas-turbine spray combustion in a constant-volume premixed combustion vessel," in *AIAA SCITECH 2023 Forum*, 2023, p. 2049.
[23] J. D. Naber and D. L. Siebers, "Effects of gas density and vaporization on penetration and dispersion of diesel sprays," *SAE Trans.*, pp. 82–111, 1996.
[24] W. J. Sim and T. E. Daubert, "Prediction of vapor-liquid equilibria of undefined mixtures," *Ind. Eng. Chem. Process Des. Dev.*, vol. 19, no. 3, pp. 386–393, 1980.
[25] J. T. Edwards, "JET FUEL PROPERTIES." Air Force Research Laboratory, AFRL-RQ-WP-TR-2020-0017, 2020.
[26] "NIST Chemistry WebBook." https://webbook.nist.gov/chemistry/
[27] "PubChem." https://pubchem.ncbi.nlm.nih.gov/
[28] D. J. Luning Prak, J. S. Cowart, and P. C. Trulove, "Density and viscosity from 293.15 to 373.15 K, speed of sound and bulk modulus from 293.15 to 343.15 K, surface tension, and flash point of binary mixtures of bicyclohexyl and 1, 2, 3, 4-tetrahydronaphthalene or trans-decahydronaphthalene at 0.1 MPa," *J. Chem. Eng. Data*, vol. 61, no. 1, pp. 650–661, 2016.
[29] T. M. Koller *et al.*, "Liquid viscosity and surface tension of n-dodecane, n-octacosane, their mixtures, and a wax between 323 and 573 K by surface light scattering," *J. Chem. Eng. Data*, vol. 62, no. 10, pp. 3319–3333, 2017.
[30] J. T. Edwards, "Reference jet fuels for combustion testing," in *55th AIAA aerospace sciences meeting*, 2017, p. 0146.
[31] L. Esclapez *et al.*, "Fuel effects on lean blow-out in a realistic gas turbine combustor," *Combust. Flame*, vol. 181, pp. 82–99, 2017.
[32] C. J. Mueller *et al.*, "Methodology for formulating diesel surrogate fuels with accurate compositional, ignition-quality, and volatility characteristics," *Energy Fuels*, vol. 26, no. 6, pp. 3284–3303, 2012.
[33] M. Colket and J. Heyne, *Fuel effects on operability of aircraft gas turbine combustors*. American Institute of Aeronautics and Astronautics, Inc., 2021.
[34] R. Lin and L. L. Tavlarides, "Thermophysical properties needed for the development of the supercritical diesel combustion technology: Evaluation of diesel fuel surrogate models," *J. Supercrit. Fluids*, vol. 71, pp. 136–146, 2012.